Total (p,π^+) cross sections on light nuclei near the pion Coulomb barrier

R. E. Marrs,* R. E. Pollock, and W. W. Jacobs
Indiana University Cyclotron Facility, Bloomington, Indiana 47405
(Received 7 May 1979)

Angle-integrated (p,π^+) cross sections on ^{9}Be, ^{10}B, ^{11}B, ^{12}C, ^{13}C, ^{14}N, and ^{16}O have been measured over the energy range $0.5 \lesssim T_p - T_{\text{threshold}} \lesssim 10$ MeV by detecting μ^+ decays. By combining the present results with higher energy measurements we show that, for $1p$-shell targets, the energy dependence of the (p,π^+) reaction from $T_\pi \approx 0.5$ to ≈ 50 MeV can be explained in terms of pion phase space and barrier penetration.

[NUCLEAR REACTIONS ^{9}Be$(p,\pi^+)^{10}$Be, ^{10,11}B$(p,\pi^+)^{11,12}$B, ^{12,13}C$(p,\pi^+)^{13,14}$C, ^{14}N$(p,\pi^+)^{15}$N, and ^{16}O$(p,\pi^+)^{17}$O, $T_p - T_{\text{threshold}}$: 0.5–10 MeV, measured angle-integrated cross sections.]

I. INTRODUCTION

Recent measurements of (p,π^+) angular distributions on complex nuclear targets[1-4] and the expectation of more data in the near future have stimulated numerous theoretical investigations of the (p,π) reaction mechanism and a few calculations of its energy dependence.[5-8] The attention currently being given to this reaction is due in part to the fact that a complete theory of pion production near threshold remains elusive and in part to the hope that, once understood, the (p,π) reaction may provide new nuclear structure information.

Measurements of the energy dependence of (p,π^+) cross sections below the (3, 3) resonance can provide an important constraint for models of pion production. Angular distribution data for several different targets and final state configurations are now becoming available in this range of proton energies.[4] The present study of angle-integrated (p,π^+) cross sections near and below the π^+ Coulomb barrier extends our knowledge of the (p,π^+) reaction to the lowest possible pion energies. By combining the present results with recent higher energy measurements[4] we study angle-integrated ground-state (p,π^+) cross sections on $1p$ shell targets over the range of pion energy from $T_{\pi^+} \approx 0.5$ MeV to ≈ 50 MeV. Data over such a large energy range near threshold, for which phase space and barrier penetration effects can be easily removed, may allow one to explore interesting features of the intrinsic pion production mechanism. Alternatively, an extrapolation of these data can provide a measure of (p,π^+) reaction strengths in the zero-pion-energy limit.

At energies near threshold ($T_{\pi^+} \lesssim 50$ MeV) the pion wavelength is larger than the radii of light nuclei, and only a few pion partial waves contribute to the (p,π^+) reaction. The energy dependence of the reaction arises mainly from the following effects:

(1) pion phase space,

(2) pion Coulomb and centrifugal barrier penetration,

(3) nuclear distortion of the pion and proton wave functions,

(4) explicit energy dependence of the production operator.

A phenomenological interpretation by Gell-Mann and Watson,[9] which accounts for effects (1) and (2), has been successfully applied to the simplest (p,π^+) reaction, $pp \to \pi^+ d$.[10-12] In this model the cross section is written as $\sigma_{\text{total}} = G_0 \alpha \eta + G_1 \beta \eta^3$, where the two terms correspond to the incoherent contributions of $l=0$ and $l=1$ pion partial waves to the angle-integrated cross section; α and β are constants, G_0 and G_1 are Coulomb factors, and $\eta = p_\pi(\text{c.m.})/m_\pi c$. We examine the extent to which (p,π^+) excitation functions on complex nuclei can be fitted with simple phenomenological expressions of this form, which account for phase space and nuclear penetrability but suppress the energy dependence of the production mechanism. More sophisticated calculations are beyond the scope of the present paper.

II. DESCRIPTION OF THE EXPERIMENT

A. Experimental Details

Inclusive (p,π^+) total cross sections were measured by detecting the energetic positrons from $\pi^+ \to \mu^+ \to e^+$ decay. Proton beams at several energies between 138 and 154 MeV were obtained from the Indiana University isochronous cyclotrons. The proton beam energy was determined from the field in a momentum analysis magnet to an accuracy of ±120 keV. The analyzing magnet calibration was derived from standard (p,d) and (p,t) crossover measurements at 36- and 62-MeV pro-

ton energy obtained with the Indiana quadrupole-dipole-dipole-multipole (QDDM) magnetic spectrograph. The accuracy of the extrapolation of the calibration to higher analyzing magnet fields was confirmed with field maps of the magnet and by QDDM measurements of (p,π^+) cross sections close to threshold.[4]

Electrostatic deflection plates located between the two cyclotrons were used to obtain proton beam bursts of approximately 1 μs duration at a typical repetition rate of 60 kHz. Pions and the muons into which they decay were stopped in aluminum near the target as illustrated in Fig. 1. The scattering chamber consisted of a section of thin-walled aluminum tubing, and targets were accommodated in a vertical cross member. For most of the measurements the chamber and cross member were reinforced to a total thickness of 2.4 mm of aluminum, which was sufficient to retain all muons produced from proton beams up to 8 MeV above threshold. For a few measurements at higher energies an additional 6.4 mm of aluminum was added.

The μ-decay positrons were counted immediately after the beam bursts in a stack of three 1.27-cm thick plastic Čerenkov counters and one 0.64-cm thick scintillation counter. Each counter was covered by 3.2 mm of aluminim in order to decouple the counters for low-energy events. The 12.7 $\times$ 12.7-cm scintillator defined a solid angle of 76

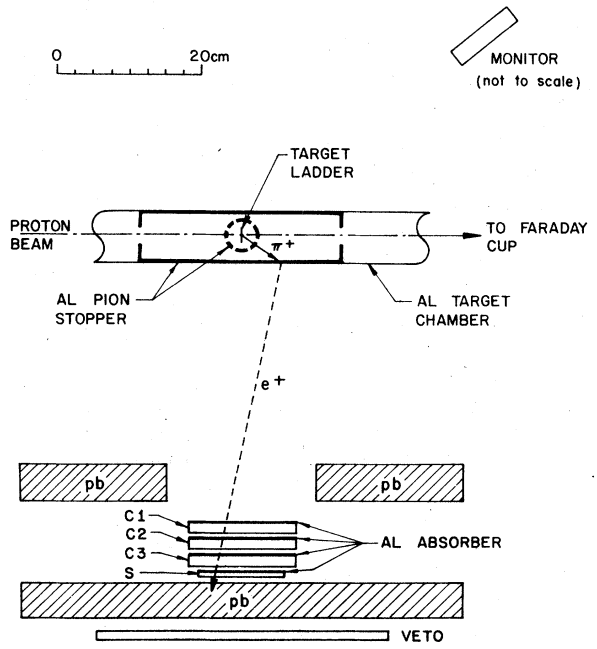

FIG. 1. Schematic layout of the experiment. C1-C3 are plastic Čerenkov counters. *S*, veto, and monitor are plastic scintillators.

msr. The three Čerenkov counters consisted of 15.2$\times$15.2-cm Pilot 425 Čerenkov material, which contains a wavelength shifter. The Lucite light guides extended in different directions and were mostly shielded from the target by lead. RCA 8575 photomultiplier tubes were used for all of the counters. Events were defined by a fast 4-fold coincidence using commercial electronics modules, and the pulse heights from the four counters were saved on magnetic tape along with the time of the event with respect to the beam burst.

A veto scintillation counter located behind 5 cm of lead (see Fig. 1) rejected cosmic rays with 90% efficiency and had a negligible response to μ-decay events. The time profile of the beam was monitored with a 10-cm deep plastic-scintillator charged-particle counter situated at approximately 40° and 1.5 m from the target. Monitor events were tagged and recorded along with the coincidence events. A single time-to-amplitude converter (TAC) was driven by both the monitor and coincidence events.

The time spectrum from the highest-yield run is shown in Fig. 2(a), and a run at an energy only 500 keV above the (p,π^+) threshold is shown in Fig. 2(c). The quality of the beam burst is illustrated by the monitor time spectrum shown in Fig. 2(b). The average proton current was collected in a Faraday cup and integrated. Total (p,π^+) cross sections were extracted by numerically integrating over the monitor TAC peak weighted by e^{t/τ_μ}. This method correctly accounts for μ decay during the beam burst, which varied slightly in arrival time and shape. Time-averaged beam currents varied between 5 and 20 nA.

Figure 3 shows pulse height spectra in the Čerenkov counters corresponding to μ-decay events [same run as Fig. 2(a)]. The Čerenkov-counter pulse heights were summed in pairs by software, and events in the low-energy tails of these spectra and the scintillator spectrum were removed by software cuts in order to reduce the background. This procedure reduced the number of prompt events by a factor of 4.

Instantaneous singles rates in the four coincidence counters typically ranged from 0.1 to 1.0 MHz during the beam-on phase and from 3 to 20 KHz during the beam-off phase. Most of the coincident background during the beam-off phase can be attributed to cosmic rays. The prompt peak in the TAC spectrum could be accounted for by events consisting of a real coincidence between at least two counters and a random coincidence with the other counters. Most of the beam-associated background is attributed to γ-ray induced events. Total coincidence rates were usually less than 100 Hz, and a correction for computer deadtime

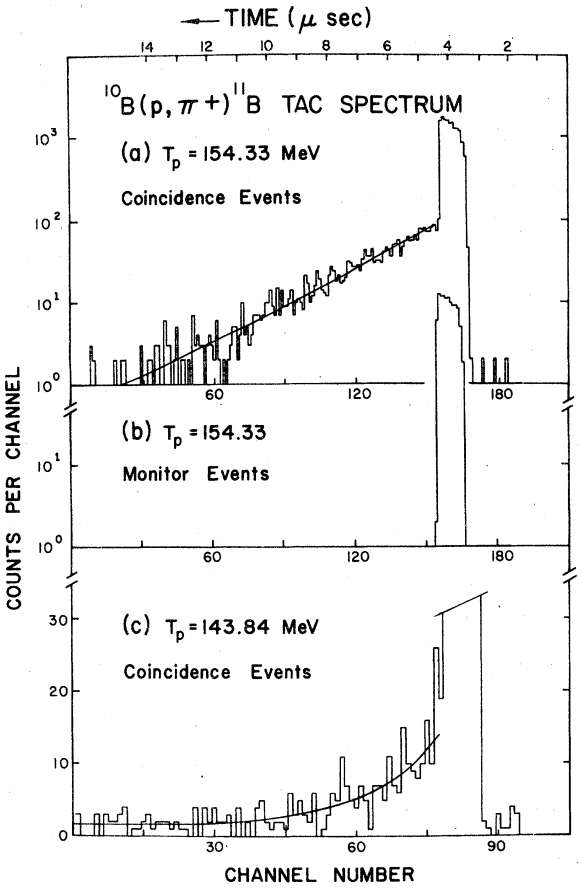

FIG. 2. Extreme examples of the data. (a) TAC spectrum from a ^{10}B target 10 MeV above the (p,π^+) threshold. (b) Monitor TAC spectrum from the same run. (c) TAC spectrum from a ^{10}B target 500 keV above the (p,π^+) threshold. Smooth curves are least-squares fits.

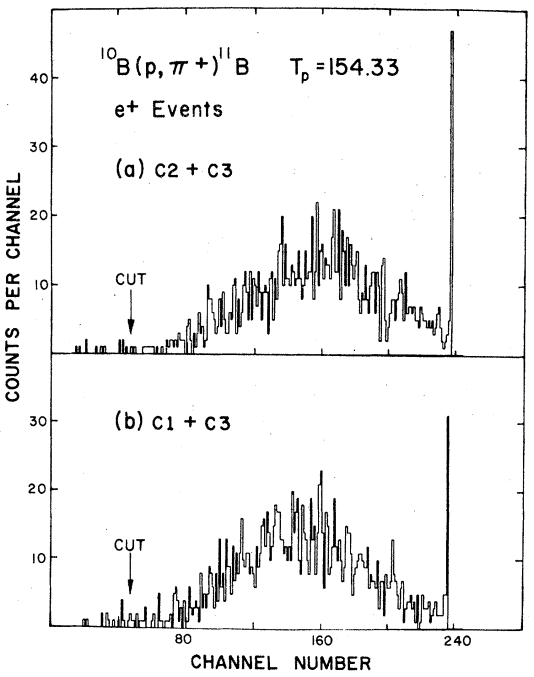

FIG. 3. Pulse height spectra from the three Čerenkov counters summed in pairs and gated by delayed events. The peak just below channel 240 corresponds to electronic saturation.

(usually less than 2%) was made by scaling the number of fast coincidences.

The smooth curves in Fig. 2 are least-squares fits to a 2.2-μs exponential decay plus a constant background. The fitting program, which was applied to all of the data, combined channels in the low-counts region of the TAC spectra and was constrained to reproduce the total number of delayed events in order to reduce the bias inherent in least-squares fits to low-statistics data. All of the fits yielded a reduced χ^2 close to one.

B. Efficiency Calculation

The efficiency of the apparatus for detecting μ^+ decays was less than 100% due to the failure of low-energy positrons to penetrate the detector stack, annihilation in flight, and other effects which are discussed below.

The fraction of the μ-decay positron spectrum accepted by the detector stack was computed from tables of electron ranges and stopping powers[14] assuming a positron spectrum of the form $N(x)dx = (6x^2 - 4x^3)dx$, where $x = 2E_{e^+}/M_\mu$. The threshold positron energy for the full detector stack was $\approx$19 MeV. The corresponding efficiency factor appears in Table I along with those for other effects

TABLE I. Contributions to the positron detection efficiency and its uncertainty.

Effect	Efficiency factor
e^+ spectrum cutoff	$0.92 \pm 3\%$
Annihilation in flight	$0.93 \pm 3\%$
Čerenkov counter efficiencies	$0.97 \pm^{3}_{5}\%$
Extended size of e^+ source	$1.00 \pm 2\%$
Solid angle uncertainty	$1.00 \pm 4\%$
Veto counter false rejection	$0.99 \pm^{1}_{3}\%$
e^+ multiple scattering in counters	$0.97 \pm 2\%$
Holes at 0° and 180°	negligible effect
Shadowing by target assembly	negligible effect
μ^+-e^+ directional correlation	negligible effect
π^+ interaction before decay	negligible effect
Total efficiency	$0.80 \pm 9\%$

considered below. The probability of annihilation in flight before reaching the last counter was computed by folding the known annihilation cross sections[15] into the positron spectrum.

The product of the individual efficiencies of the three Čerenkov counters was determined by removing them from the fast coincidence one at a time while running a high-yield target and proton energy, and also by sorting data with and without the software cuts on the Čerenkov pulse heights. The scintillation counter was assumed to have 100% effficiency.

The geometrical $(1/r^2)$ effects of different π^+ angular distributions and the extended e^+ source size were estimated by numerically integrating over the cylindrical shape of the pion stopper folded with observed (p,π^+) angular distributions.[4] Several other effects estimated in a less rigorous manner are also summarized in Table I.

III. RESULTS

Our angle-integrated cross section measurements are plotted in Figs. 4–10 as a function of proton kinetic energy in the laboratory. Each error bar includes both the statistical error and the uncertainty in the target thickness and uniformity. There is an additional 9% overall uncertainty in the normalization of the experiment as given in Table I.

The properties of the targets are listed in Table II. The target thicknesses were determined by weighting, and the stability of the LiOH and melamine targets was checked by repeating one run with a displaced beam spot position. The chemical composition of the LiOH target was verified by heating it in a vacuum and reweighting. The ^{11}B cross sections were corrected for the contribution from the ^{10}B impurity in the target, and the higher-energy ^{14}N cross sections were corrected for the ^{12}C component in the melamine target. Every target was run at at least one energy below threshold and a muon yield consistent with zero was observed.

Because of the rapidly changing slope of the (p,π^+) cross sections near threshold and the proton energy loss of several hundred keV in some of the targets, we define an effective energy E_{eff} for each datum point as the energy at which the true cross section assumes its observed target-averaged value:

$$\sigma(E_{\text{eff}})=\langle\sigma(E)\rangle\equiv\frac{1}{\Delta E}\int_{E_B-\Delta E}^{E_B}\sigma(E)dE,$$

where E_B is the beam energy and ΔE is the proton energy loss in the target. To determine E_{eff} we assume that the (p,π^+) cross sections have the

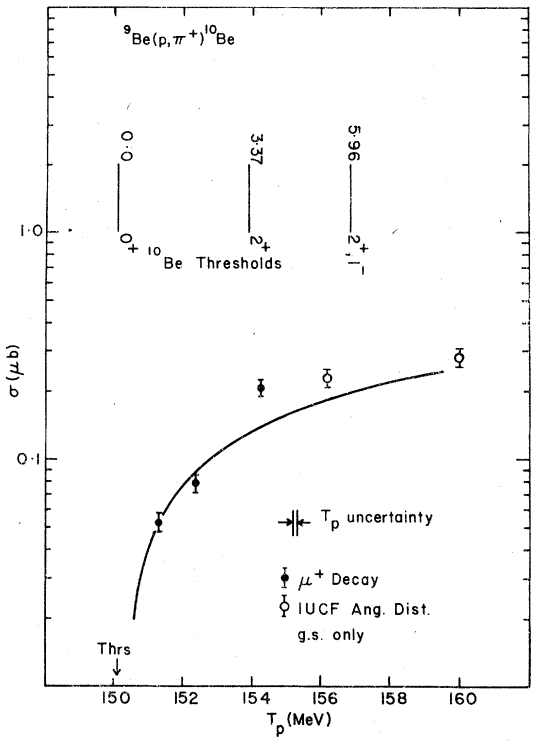

FIG. 4. Angle-integrated (p,π^+) cross sections for ^{9}Be. The solid points are inclusive data and the open points are the ground-state cross sections from Ref. 4. The curve is a Coulomb factor for the ground state (see text).

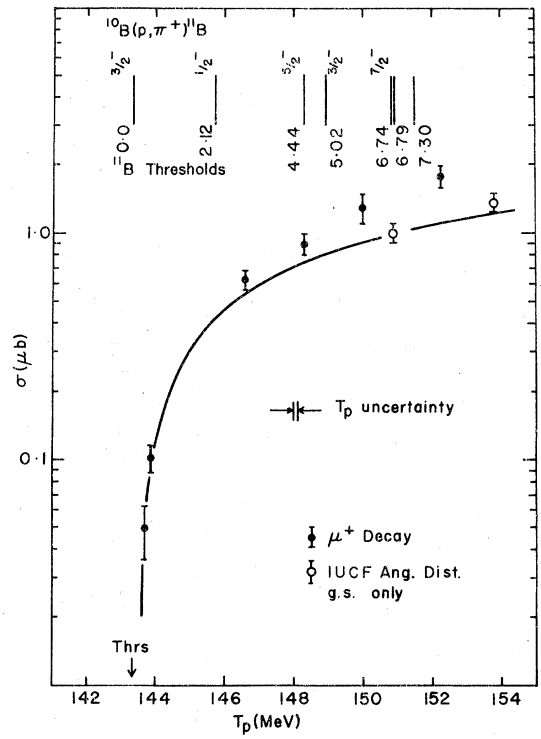

FIG. 5. ^{10}B data (see Fig. 4 caption).

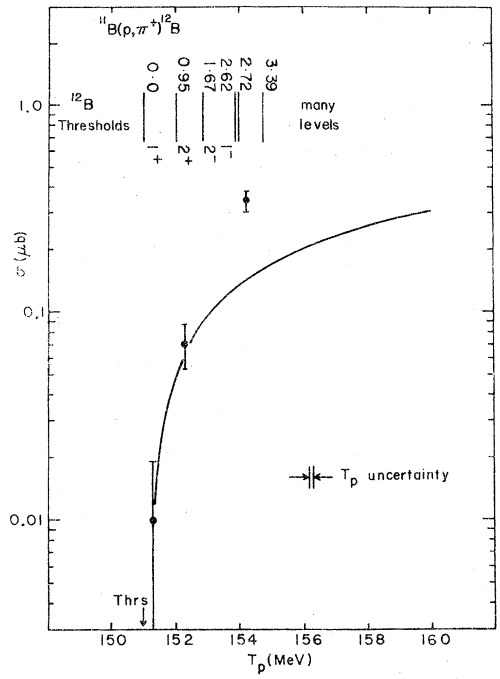

FIG. 6. ^{11}B data (see Fig. 4 caption).

shape $\sigma(p,\pi^+)\propto(k_\pi/k_p)S(k_\pi)$, where $\hbar k_\pi$ and $\hbar k_p$ are the center-of-mass momenta and $S(k_\pi)$ is the Coulomb factor discussed below. This shape was numerically integrated over the proton energy range spanned by each target in order to find the appropriate effective energy. The effective energy differed from the target-center energy by more than 20 keV only for the lowest-energy ^{10}B datum point, for which a correction of +30 keV was made, and

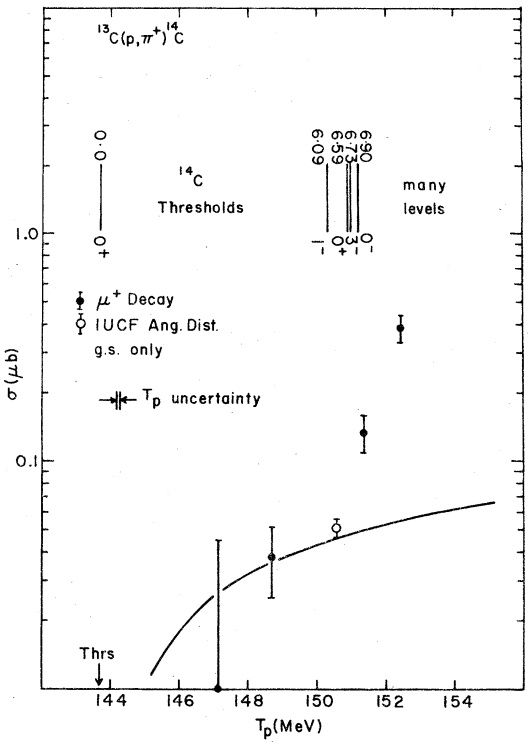

FIG. 8. ^{13}C data (see Fig. 4 caption).

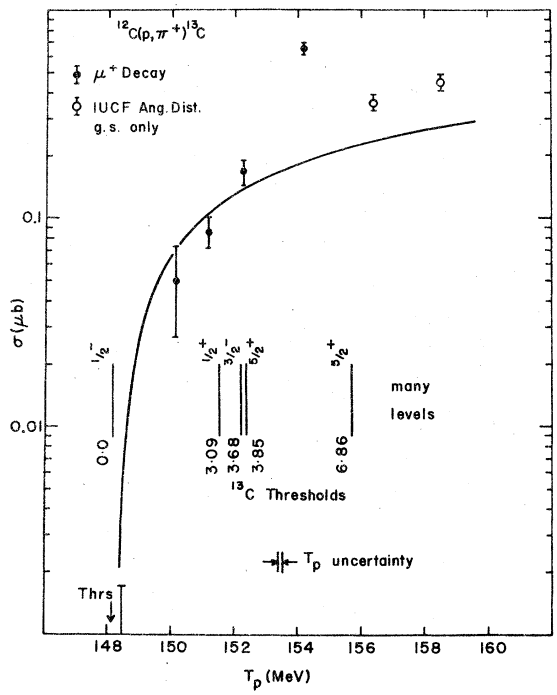

FIG. 7. ^{12}C data (see Fig. 4 caption).

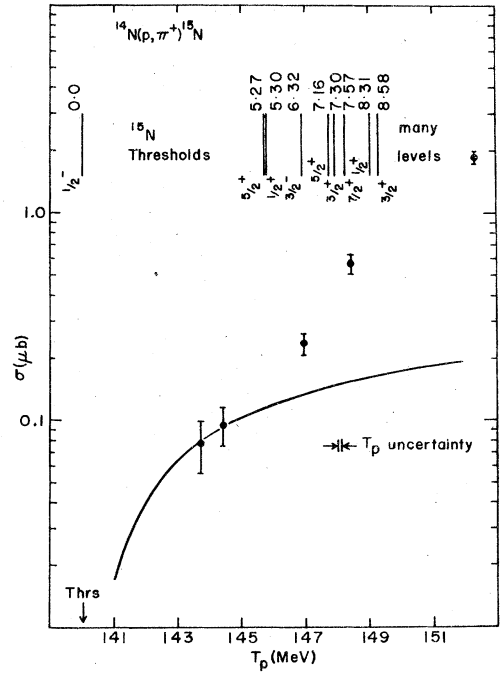

FIG. 9. ^{14}N data (see Fig. 4 caption).

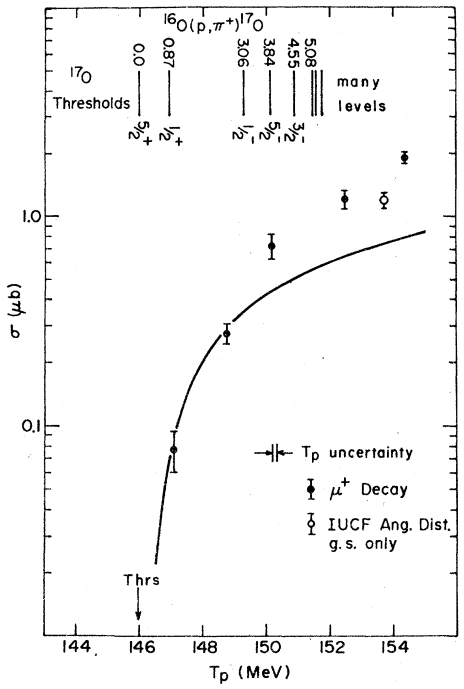

FIG. 10. ^{16}O data (see Fig. 4 caption).

for the lowest-energy ^{12}C datum point, for which a correction of +60 keV was made.

In order to study the ground-state (p,π^+) cross sections over an energy range above the excited state thresholds, we have taken data from other experiments at the Indiana University Cyclotron Facility (IUCF),[4] from previous Uppsala measurements,[1] and from recent work at TRIUMF.[2] Angle-integrated cross sections were extracted from these angular distribution measurements by least-squares fitting the data with a Legendre polynomial expansion, which is appropriate when only two or three pion partial waves contribute.

IV. DISCUSSION AND CONCLUSIONS

The (p,π^+) differential cross section in the center of mass is given by

$$\frac{d\sigma}{d\Omega}(p,\pi^+)=\frac{1}{(2\pi)^2}E_p E_\pi \frac{k_\pi}{k_p}\frac{E_A E_{A+1}}{E^2_{\text{total}}}\frac{1}{2}\frac{1}{(2S_A+1)}$$

$$\times\sum_{if}|\langle f|H|i\rangle|^2$$

in standard notation, where A refers to the target and $A+1$ to the residual nucleus. At energies near the pion Coulomb barrier the energy dependence of the production matrix element should be largely determined by the nuclear penetrability of the pion wave function. We examine the validity of this assumption by comparing the data with simple expressions for the "trivial" effects of barrier penetration and phase space. This is easy because (p,π^+) cross sections on $1p$-shell nuclei are dominated by $l=0$ and $l=1$ pion partial waves for the low pion energies considered here. For example, the nuclear penetrability evaluated at the surface of ^{10}B using pure Coulomb wave functions and 10-MeV pions is a factor of 19 smaller for $l=2$ pions than for $l=0$; and the shapes of (p,π^+) angular distributions near threshold can be reproduced with a Legendre polynomial expansion including terms no higher than $P_2(\cos\theta)$.

In Figs. 4–10 the solid curves are the expression $\sigma(p,\pi^+)=f(k_\pi/k_p)S(k_\pi)$, where the constant strength factor f has been chosen arbitrarily for each target. The Coulomb factor, $S(k_\pi)=2\pi\gamma/[\exp(2\pi\gamma)-1]$ with $\gamma=z(e^2/\hbar c)(1/\hbar c)(E_\pi/k_\pi)$, is the usual expression for the intensity of a Coulomb wave function at the origin. This is the expected energy dependence of the ground-state cross section near the pion Coulomb barrier if the energy dependence of the production operator and the nuclear distortions is small. It can be seen from Figs. 4–10 that for ^9Be, ^{10}B, ^{12}C, and ^{16}O the energy dependence of the ground-state cross sec-

TABLE II. Summary of targets used in the total cross section measurements.

Nucleus	Target material	Mass fraction of target	Total thickness (mg/cm^2)
^9Be	Metallic Be	100%	91 ± 1.5%
^{10}B	Scintered ^{10}B	96.2%	61 ±10%
			154 ±10%
			165 ±15%
^{11}B	Scintered ^{11}B	97.2%	110 ±10%
^{12}C	Natural graphite	98.9%	127 ± 5%
	Enriched graphite	100%	54.8 ± 5%
^{13}C	Enriched graphite	97%	65 ±10%
^{14}N	$C_3H_6N_6$ (melamine)	66.4%	95 ± 5%
^{16}O	LiOH	66.7%	51.3 ± 5%

tions is in fact determined primarily by phase space and barrier penetration. The data for the other targets (^{11}B, ^{13}C, ^{14}N) and for the excited state yields (derived by subtraction of the ground-state yield curves) cover too small an energy range to permit drawing a similar conclusion. However, if we assume that barrier penetration and phase space determine the energy dependence of all (p,π^+) cross sections within 10 MeV of threshold, then the present data can provide a measure of the strength of $\sigma(p,\pi^+)$ for all of the ground states as well as several excited states. This information is useful both as a constraint for calculations of nuclear structure effects in the (p,π) reaction and as a guide for future (p,π^+) angular distribution measurements. In particular, our data provide a measure of (p,π^+) reaction strengths in the zero-pion-energy limit now that the energy dependence at threshold has been determined.

Now let us consider a larger range of pion energy, up to $\approx$50 MeV above threshold. All available angle-integrated (p,π^+) ground-state cross sections for $1p$-shell targets are plotted in Fig. 11 as a function of pion wave number. The data points obtained from Uppsala angular distributions have been multiplied by 1.5 to account for a normalization discrepancy[4] and arbitrarily assigned 20% uncertainties for plotting purposes.

For comparison, data for the $pp\to\pi^+d$ reaction over the same range of pion momentum are also shown in Fig. 11. The lower momentum hydrogen data were obtained from the $\pi^+d\to pp$ data of Rose[13] by applying detailed balance:

$$\sigma(pp\to\pi^+d)=\frac{3}{2}\,\frac{k_\pi^{\,2}}{k_p^{\,2}}\,\sigma(\pi^+d\to pp).$$

The solid curve through the hydrogen data in Fig. 11 is the phenomenological expression

$$\sigma(p,\pi^+)=\frac{k_p(\text{thresh})}{k_p}(\alpha\eta+\beta\eta^3)S(k_\pi),$$

where S is the Coulomb factor defined above, $\eta=(\hbar c/m_\pi c^2)k_\pi^{\text{c.m.}}$, $\alpha=0.188$ mb, and $\beta=1.035$ mb. The η and η^3 terms correspond to the contributions of $l=0$ and 1 pion partial waves, respectively. This curve is fit 1 of Richard-Serre, *et al.*[11] with their value of β increased by 15% to compensate for the explicit k_p dependence in our expression. (Our Coulomb factor S does not differ significantly from the G_0 and G_1 of Refs. 11 and 12 over the energy range shown in Fig. 11.) The $pp\to\pi^+d$ reaction can clearly be fitted with this type of phenomenological expression, and the fit continues to work at higher energies.[11] Now let us see how well the same approach works for complex nuclei over the same pion momentum range.

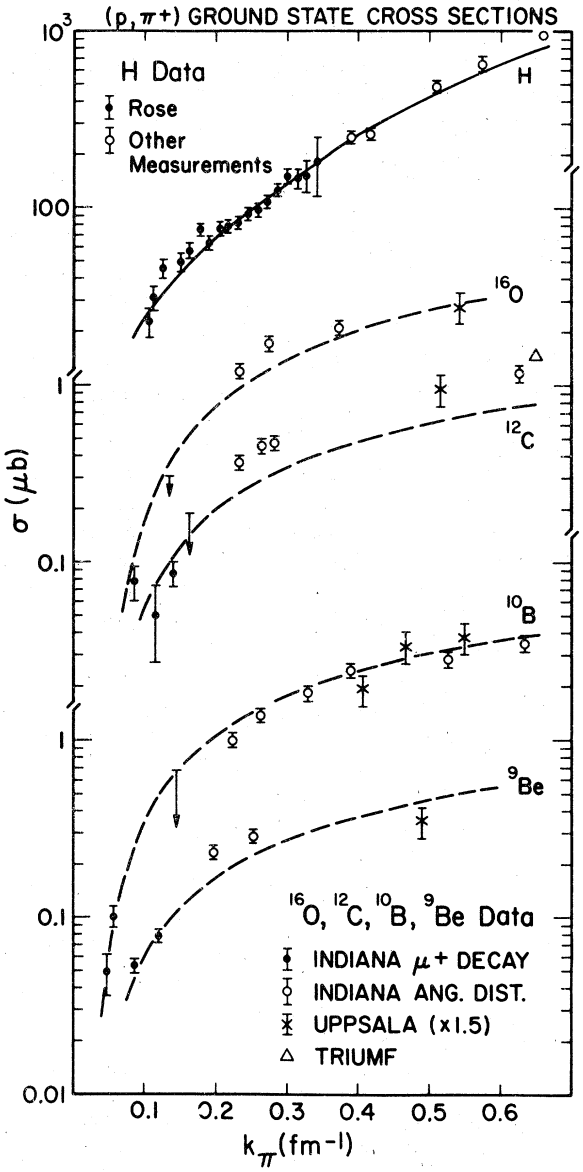

FIG. 11. Ground-state (p,π^+) cross sections plotted vs pion wave number in the center of mass. Some inclusive measurements above the first-excited-state threshold are shown as upper limits. The broken curves are a simple Coulomb factor (see text). The hydrogen data are from Refs. 13, 11, and references therein, and the solid curve is a phenomenological expression explained in the text.

The broken curves shown with the ^{9}Be, ^{10}B, ^{12}C, and ^{16}O data in Fig. 11 are the simpler expression (i.e., $\beta=0$) which was used in Figs. 4–10. Although the different energy dependence of s and p wave penetrabilities is neglected in this expression, which evaluates Coulomb wave functions at the origin, the Coulomb factor $S(k_\pi)$ has a shape intermediate between that of $l=0$ and $l=1$ surface

Coulomb penetrabilities for the range of energies and targets considered here.

It can be seen that the (p,π^+) ground-state cross sections in Fig. 11 exhibit an energy dependence similar to the broken curves, indicating the dominant influence of pion phase space and barrier penetration effects for production from light targets up to 50 MeV above threshold. There is some indication that for the ^{12}C target the cross section rises more rapidly with energy, up to about 12 MeV ($k_\pi = 0.3$ fm^{-1}), than for the other targets. The energy dependence of $l=0$ and 1 penetrabilities is quite different in this energy range. Hence one would expect some variation from target to target in the energy dependence of the cross section if the relative $l=0$ and $l=1$ pion partial wave amplitudes vary. For example, the ^{10}B target produces $l=0$ pions for protons of $l=2$ and $l=4$, while for a ^{12}C target the $l=0$ pions can be produced only by protons of $l=0$. Postulating a yield increasing as $(2l_p+1)$ would account qualitatively both for the higher yield from ^{10}B and for the steeper energy dependence from ^{12}C (fewer $l=0$ pions). When higher energy angular distributions for resolved final states from targets of ^{11}B, ^{13}C, and ^{14}N become available, it will be possible, by combining these with the data in Figs. 6, 8, and 9, to complete this light-target survey of the energy dependence of the (p,π^+) reaction in the near-threshold region.

Angular distributions contain additional information about the relative magnitudes for the lowest proton partial waves. In combination with the energy dependence of the angle-integrated cross sections presented here, for which the barrier penetration and phase space effects can be removed with some degree of model independence, it will be possible to make a more precise statement about the apparent energy independence of the intrinsic pion production process which is emerging from the near-threshold measurements on light nuclei. It is, however, beyond the scope of the present paper to pursue this point. It is sufficient to state that a model of the production process will be greatly constrained by these measurements. In particular, plane-wave calculations in the one-nucleon model[6,7] assume a pion production operator proportional to $[\vec{k}_\pi - \lambda(m_\pi/m_p)\vec{k}_p]$. In the static ($\lambda=0$) limit this operator adds an additional factor of k_π^2 to the broken curves of Fig. 11, which is not consistent with the data.

ACKNOWLEDGMENTS

The authors thank R. D. Bent *et al.* and B. Hoistad *et al.* for permission to use their data prior to publication. One of us (R.E.M.) acknowledges the support and hospitality of the University of British Columbia during the preparation of this manuscript. This work was supported in part by the National Science Foundation under Grant No. PHY 78-22774.

*Present address: University of Washington, Seattle, Washington 98195.

[1]S. Dahlgren, P. Grafstrom, B. Hoistad, and A. Asberg, Nucl. Phys. A227, 245 (1974), and references therein.
[2]E. G. Auld, A. Haynes, R. R. Johnson, G. Jones, T. Masterson, E. L. Mathie, D. Ottewell, P. Walden, and B. Tatischeff, Phys. Rev. Lett. 41, 462 (1978).
[3]R. D. Bent, P. T. Debevec, P. H. Pile, R. E. Pollock, R. E. Marrs, and M. C. Green, Phys. Rev. Lett. 40 495 (1978).
[4]P. H. Pile, Ph.D. thesis, Indiana University, 1978 (unpublished), and P. H. Pile, R. D. Bent, R. E. Pollock, P. T. Debevec, R. E. Marrs, M. C. Green, T. P. Sjoreen, and F. Soga, Phys. Rev. Lett. 42, 1461 (1979).
[5]M. P. Keating and J. G. Wills, Phys. Rev. C 7, 1336 (1973).
[6]J. V. Noble, Phys. Rev. Lett. 37, 123 (1976).
[7]R. Brockmann and M. Dillig, Phys. Rev. C 15, 361 (1977).
[8]L. D. Miller and H. J. Weber, Phys. Rev. C 17, 219 (1978).
[9]M. Gell-Mann and K. Watson, Annu. Rev. Nucl. Sci. 4, 219 (1954).
[10]J. Spuller and D. F. Measday, Phys. Rev. D 12, 3550 (1975).
[11]C. Richard-Serre, W. Hirt, D. F. Measday, E. G. Michaelis, M. J. M. Saltmarsh, and P. Skarek, Nucl. Phys. B20, 413 (1970).
[12]A. Reitan, Nucl. Phys. B11, 170 (1969).
[13]C. M. Rose, Phys. Rev. 154, 1305 (1967).
[14]M. J. Berger and S. M. Seltzer, NASA SP-3012 (1964).
[15]W. Heitler, *Quantum Theory of Radiation* (Oxford University Press, London, 1954).